Monitoring Atom Traps for

Neutral Atom Quantum Computing

A Senior Project

presented to

the Faculty of the Physics Department

California Polytechnic State University, San Luis Obispo

In Partial Fulfillment

of the requirements for the Degree

Bachelor of Science

by

Taylor Shannon

March, 2014

Table of Contents

List of Figures

1. **Introduction**

Moore's law was an observation made in the 1960's by George Moore that the number of transistors per square inch on integrated circuits doubles every two years due to improvements in technology [1]. While this law has proved generally correct since then, there is a limit to the amount of transistors one can put on a single chip because one cannot make a transistor smaller than the size of an atom. According to IBM, one bit of data is currently stored using about one million atoms, but a twelve atom bit is being developed [2]. Therefore, these few atoms will be used to represent either a logical "0" or "1" state. However, there is another use for the atom that could bring the power of computing to a whole new level.

Quantum observables, such as energy, within atoms can be exploited to increase the amount of information represented by atoms. In contrast to a standard bit which exists in one of two states ("0" or "1"), an atom can exist in a superposition of two states. This allows the number of inputs for an n-bit system to change from 1 to 2^n. Instead of twelve atoms allowing one input, superposition permits twelve atoms to allow 2^{12}, or 4096, inputs. In this case, the atoms are referred to as quantum bits, or qubits. The successful construction of a many qubit quantum computer will lead to a drastic leap in certain computational matters such as encryption. It would also increase the capability of simulating quantum systems and many-body systems in a timely manner which could lead to improved technology and a greater understanding of the universe.

Single qubits have been created, but a quantum computer requires a large system of qubits ($\sim 10^6$) as well as gates to perform logic, which requires quantum entanglement. One area of research that involves using atoms as qubits and has been shown to be a feasible method of creating a quantum computer is neutral atom quantum computing [3]. Neutral atom quantum

computing uses the electronic or motional states of neutral atoms as qubits. Neutral atoms are ideal candidates because they currently satisfy four of the five DiVincenzo criteria for creating a practical quantum computer. These five criteria include the ability to initialize qubits into an initial state, long coherence time, accurate quantum gate operation, readability, and scalability [4]. To trap neutral atoms, one may use an optical dipole trap which utilizes the interaction of light with the atom's induced dipole moment [5]. Once trapped, the atom can be prepared in a desired initial state using standard techniques of laser spectroscopy [6]. Neutral atoms in their ground state are poorly coupled to the environment, so their coherence time is longer than other proposed qubits such as ions [3]. The construction of two-qubit gates is possible, and to do so it is advantageous to be able to bring two atoms together. Since the hyperfine states of neutral trapped atoms are well characterized, the quantum state may be easily read using spectroscopic techniques.

Neutral atoms thus currently satisfy four of the five DiVincenzo criteria. The remaining obstacle for neutral atom quantum computing is scalability. Since the atomic interaction between neutral atoms is relatively weak, it is easy to trap and cool atoms in large numbers in a three-dimensional array [3]. However, a technique to interact with one atom without disturbing the state of the others is essential. Gillen *et al.* have proposed a two-dimensional array of dipole traps that allows each atom to be individually addressed, without disturbing the surrounding atoms [7]. By shining laser light on a pinhole, a diffraction pattern is produced immediately behind the pinhole. This diffraction pattern contains local intensity maxima and minima, known as bright and dark spots, respectively. Gillen *et al.* have shown computationally that atoms can be trapped in these localized bright and dark spots [8]. By shining light through multiple pinholes, a two dimensional array of trapped atoms may be created in a manner that allows individual atoms to

be addressed and manipulated in order to perform operations [7]. The system is scalable, meaning that we can scale up to the required $\sim 10^6$ qubits required to sustain a quantum computation with error correction.

In this system, the atoms are first cooled using a magneto-optical trap (MOT), and then are transferred to the dipole traps. During this transfer, the MOT is quickly turned off on the order of $\sim$10 milliseconds, and the diffraction pattern is immediately projected onto the atom cloud. During this short process and the time that the atoms are in the dipole traps (we expect on the order of ~100 milliseconds), the atoms must be monitored to ensure they were successfully transferred to the trap. This is done by an imaging system that consists of a high speed camera and a photodiode. Using the imaging system, we can also determine the temperature and number of atoms in the MOT and dipole traps, as well as measure the trap frequency. This paper will explain the creation and implementation of this part of the experiment.

2.   Background of the Magneto-Optical Trap

2.1. Doppler Cooling

Before the neutral atoms may be loaded into atomic dipole traps, a magneto-optical trap (MOT) is used to cool them. For this experiment, Rubidium-87 atoms are placed under ultra-high vacuum at room temperature and are cooled down to the ~100 μK range by a process called Doppler cooling. When an atom absorbs a photon, it receives a momentum kick equal to the momentum of the absorbed photon, in the direction that the photon was traveling. After a short time, the atom re-emits the photon in a random direction. These random directions cancel out on average, and the atom receives a net momentum shift in the direction of incoming photons. Note

that if the atom is moving towards the light source, it perceives higher frequency (higher energy) photons due to the Doppler Effect, shown in Figure 1. Doppler cooling involves adjusting the frequency of incoming photons produced by a laser to just below the resonant frequency of an electronic transition of the atom. This adjustment is referred to as detuning the laser, and light detuned below the resonant frequency is referred to as being red detuned. When an atom is moving towards the red detuned light, the photons are closer to resonance with the atom's electronic transition due to the Doppler Effect, so the probability of the atom absorbing a photon increases. With each absorption, the atom loses momentum equal to the momentum of the photon. As the atom slows down, it will absorb fewer photons because the light will be further from resonance. This slowing process decreases the kinetic energy of the atoms and therefore cools them. The atoms must experience this laser cooling from all directions to be sufficiently slowed down. If an atom is at rest in this red detuned laser light, it has a probability of absorbing a photon but because the photon is below resonance, it will not happen frequently. Additionally, the atom will on average absorb the same number of photons from all directions because it is not moving toward any of the laser sources, so the net effect will be zero. The laser used for this process is referred to as the trap laser.
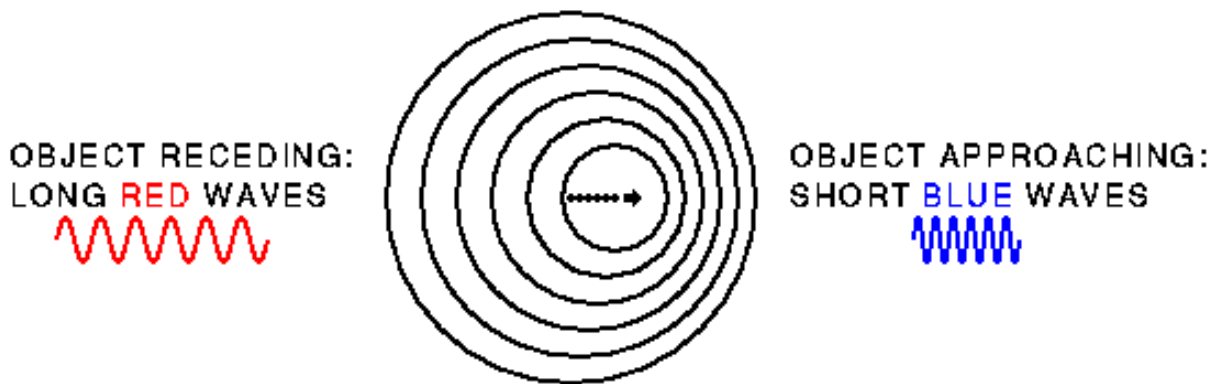

Figure 1: The Doppler Effect for light [9]

For Rubidium-87, the transition involved for cooling is the D2 transition from the F=2 hyperfine state in the $5^2S_{1/2}$ manifold to $F = 3$ in the $5^2P_{3/2}$ manifold. After roughly 26 nanoseconds, the electron will decay back down to the initial state. These transitions are shown by the blue dashed lines in Figure 2. The atom then absorbs another photon and continues to undergo this cyclic process. The more cycles that an atom undergoes, the more momentum kicks it receives and the slower the atom travels.
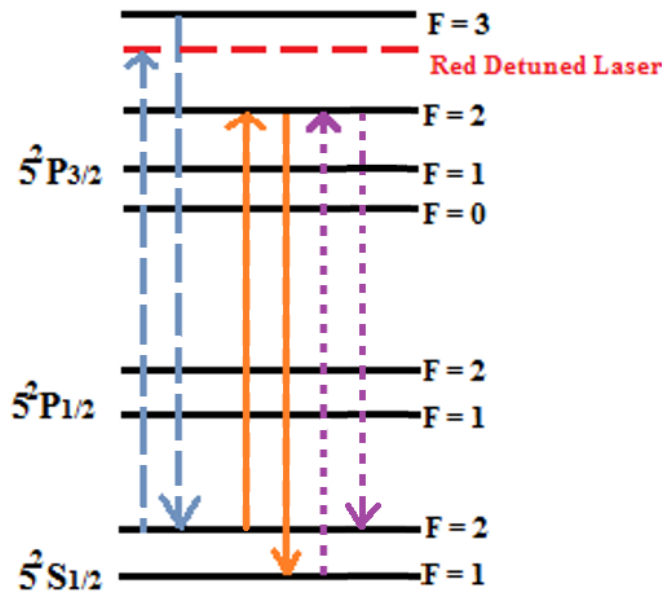
Figure 2: Hyperfine energy levels for Rubidium-87. The Doppler cooling transitions from the trap laser are shown in dashed blue. The pump laser transitions are shown in dotted purple.

If all went perfectly well, the above description would be all that is needed for Doppler cooling. However, sometimes the atom will only absorb enough energy to excite an electron to the $F = 2$ state of the $5^2P_{3/2}$ level. At this level, the atom now is allowed to decay down to the $F = 1$ state of the $5^2S_{1/2}$ manifold, instead of $F = 2$. This undesired transition is shown by the solid orange lines in Figure 2. In the lower F=1 state, the atom cannot be excited up to the required state by

the red detuned laser because there is not enough energy and the transition is forbidden by selection rules. At this point, the Doppler cooling process will not affect that respective atom. This problem is resolved with a second laser called the pump laser. The pump laser has the frequency required to excite the atom from F = 1 in the $5^2S_{1/2}$ manifold up to F = 2 in the $5^2P_{3/2}$ manifold which is shown by the dotted purple lines in Figure 2. From there it has a probability of decaying to the F=2 state of the $5^2S_{1/2}$ level again and may continue the cooling process.

2.2. Zeeman Shift and Magnetic Field

After the atoms have been slowed down by the Doppler cooling process, they must be moved to the center of the trap. This is done using polarized light and a magnetic field produced by sending current through a pair of anti-Helmholtz coils. The magnetic field between the coils is not uniform and varies roughly linearly near the center in all three dimensions. This effect in one-dimension is shown in Figure 3. When an atom is near the center of the coils, it experiences the Zeeman Effect which causes the energies of the ground state sublevels of the atom to be shifted. This energy shift varies with the atom's distance from the center due to the changing magnetic field. The change in energy due to the Zeeman Effect is given by

$$\Delta E = \mu_B g m B. \tag{1}$$

In Equation 1, B is the strength of the magnetic field, g is the Lande g-factor, μ_B is the Bohr magneton, and m is the magnetic quantum number which is dependent on the z-component of the angular momentum of the atom. As the atom moves further from the center, it experiences a greater Zeeman shift due to the increasing magnetic field.
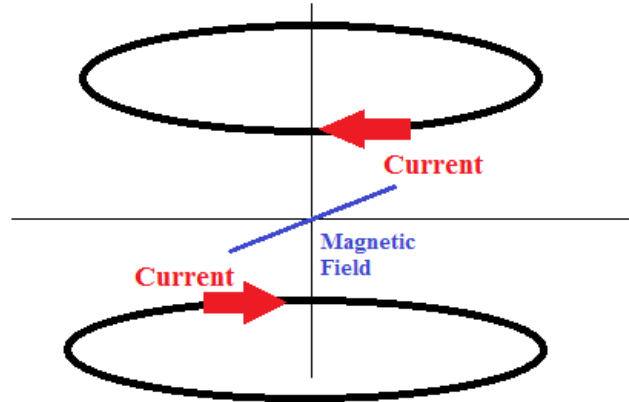
Figure 3: One-Dimensional magnetic field produced near the center of two anti-Helmholtz coils

The linearly changing magnetic field aids in pushing the atoms towards the center of the trap. In order to illustrate the basic principles behind this effect, we consider a J = 0 to J = 1 energy transition in a hypothetical simplified atom. While the example is not identical to Rubidium-87, the same basic principles apply. The magnetic field causes the $m_J = 1$ and $m_J = -1$ atomic substates to split according to Equation 1 and shown in Figure 4.

Figure 4: Zeeman splitting in magnetic field with incoming polarized photons

Imagine an atom in the J = 0 state on the right of Z_0 in Figure 4. The energy of the red detuned laser light appears close to the same energy as the J = 1, m_J = -1 line. The atom is inclined to absorb a photon to jump to that state, but can only do so if angular momentum is conserved. To ensure this requirement is fulfilled, circularly polarized light with the appropriate angular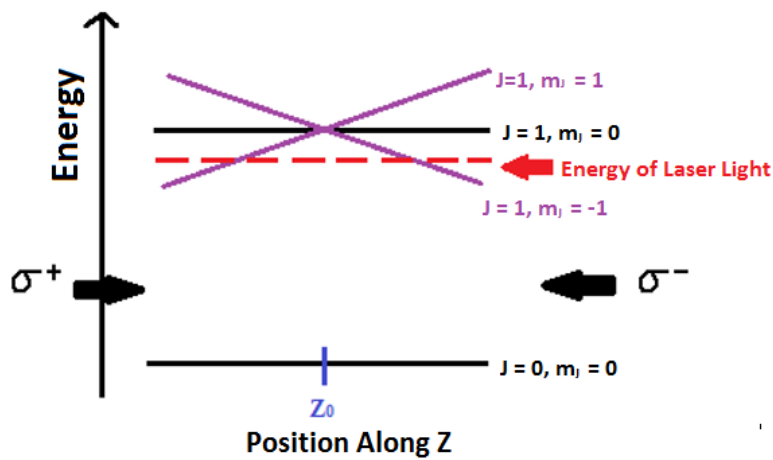 momentum value is used. A photon with angular momentum of 1 unit is referred to as σ^+, and similarly one with -1 unit is σ^-. Therefore, the atom on the right of Z_0 will be inclined to absorb σ^- polarized light because it is near resonance with the m_J = -1 line. When the atom on the right absorbs this photon, it will receive momentum going to the left towards the center of the trap. Similarly, an atom on the left side of Z_0 will absorb σ^+ light because it is near resonance with the m_J = 1 transition, and will receive a momentum kick to the right. Thus, the atom will be pushed toward the center of the trap.

Using the above techniques, the atoms are cooled and collected in an atom cloud at the center of the MOT. While in this cloud, the atoms continually absorb and emit photons, and this radiation pressure keeps the atom cloud larger than preferred. We want to trap as many atoms as possible, and if the cloud is bigger than the dipole trap projection then atoms on the outside will be lost, resulting in a lower trapping efficiency. In order to decrease the size of the cloud, the laser detuning is increased so that the atoms absorb fewer photons. At this point, the atoms are ready to be transferred to the dipole traps. The magnetic field and lasers are switched off on the order of milliseconds and the light trap is projected into the chamber. This light trap can hold the atoms, but not catch new ones. Because of this, the trap lifetime is expected to last around 100 milliseconds. To ensure the atoms are transferred successfully, we need a way to view them. For this, we designed and built an imaging system that will be described in Section 3.

3. <u>Monitoring Atom Traps:</u>

3.1 Theoretical Background of Atom Detection

While the cooled atoms are in the center of the MOT, they continuously absorb and emit photons. The emitted light is referred to as the fluorescence of the atoms. The goal of my project was to set up an imaging system that monitors the fluorescence in order to gather information about the transfer from the MOT to the dipole traps. The imaging system is to be used to determine whether the atoms were successfully trapped, calculate how many were trapped, and measure the temperature of the atoms, the trap lifetime, and the trap frequency. All of these things can be measured by monitoring the fluorescence.

The emission process is spontaneous, and emitted photons are distributed over all angles. We are able to distinguish atom fluorescence from laser light because the atoms emit light in all directions while the lasers emit light only in the direction in which they propagate. Therefore, we monitor the position of the atom cloud by tracking the location of the fluorescence. While the atoms are trapped in the dipole traps, they ideally will not fluoresce at all because the lasers are detuned (their frequency is different than the atomic resonance frequency). In order to make the atoms fluoresce so that we can locate them and ensure they were trapped, we must shine resonant light on them. One way of doing this is to shine the MOT lasers on the atoms and monitor the fluorescence with a high speed camera and photodiode. Because the atoms receive momentum during this pulse, we usually only send one pulse and then start over the entire process.

The amount of fluorescence is proportional to the number of atoms and can be measured with a photodiode. The rate at which atoms in the MOT emit photons is determined by the laser

intensity and detuning. The scattering rate, or number of photons emitted per atom per second, is given by

$$\Gamma_{scat} = \frac{\frac{I_0}{I_{sat}} \frac{\Gamma}{2}}{1 + \frac{I_0}{I_{sat}} + 4\left(\frac{\Delta}{\Gamma}\right)^2} , \qquad (2)$$

as discussed in [10]. In equation 2, $\frac{I_0}{I_{sat}}$ is the total intensity of the six MOT beams divided by the saturation intensity of Rubidium. Δ is the laser detuning given by $\Delta = \omega_L - \omega_0$ where ω_L is the frequency of the laser, and ω_0 is the resonant frequency of the electronic transition in the atom. The square factor of $\frac{\Delta}{\Gamma}$ is the laser detuning divided by the natural linewidth of Rubidium. Because this factor is in the denominator, the more detuned the laser is from the atomic transition, the lower the scattering rate. The voltage read from the photodiode is proportional to the rate at which photons hit the photodiode. Thus, we use the photodiode voltage value along with the scattering rate in order to determine how many atoms are in the trap. However, we must keep in mind that the rate at which photons hit the photodiode is reduced by the solid angle covered by the collection lens. The rate of detected photons is given by

$$\Gamma_{det} = \frac{\pi r_{lens}^2}{4\pi l_{trap}^2} \Gamma_{scat} (0.96)^2 (0.995)^2. \qquad (3)$$

In equation 3, πr_{lens}^2 is the area of the collection lens (5.23 cm²) and $4\pi l_{trap}^2$ is the surface area of the sphere of scattered photons. The radius of this sphere is the distance from the lens to the trap center (in our case 17.7 cm). By dividing the area of the lens by the surface area of the sphere of photons that reach the lens, we isolate the rate of photons hitting the lens. The factor of $(0.96)^2$ accounts for the 4% loss of photons at the reflection of the two non-AR (Anti-reflective) coated glass surfaces of the chamber [10]. At each surface of each wall of the vacuum chamber,

4% of the laser light is reflected and 96% is transmitted. The lenses used for the photodiode and camera are AR coated, so only 0.5% of the light is reflected at each surface (this information can be viewed on the spec sheet [11]). Hence the factor of $(0.995)^2$ in Equation 3. The number of atoms N in the MOT can be solved for as a function of the power incident on the photodiode:

$$N = \frac{P_{det}}{hf\Gamma_{det}}. \tag{4}$$

In equation 4, hf is the energy per photon and P_{det} is the power incident on the photodiode. The photodiode was designed so that power is proportional to voltage. This will be explained in Section 3.2.2.

We also utilize fluorescence to determine the temperature of the atom cloud using a time-of-flight (TOF) technique. In the TOF technique, we shine laser light on the atom cloud and monitor how quickly the atom cloud expands. The faster the rate of thermal expansion, the higher the temperature. Assuming that the cloud of atoms is spherically symmetric, the temperature is defined by the width of the velocity distribution of the atoms by

$$T = \frac{M}{K_B}\sigma_v^2, \tag{5}$$

as given in [12]. In equation 5, σ_v is the width of the velocity distribution, which can be inferred by the change in radius of the atom cloud over time, M is the atomic mass of Rubidium, and K_B is Boltzmann's constant. Finding the velocity distribution requires a high speed camera and a photodiode.

Lastly, we use the fluorescence of the atoms to calculate the trap frequency. Near the bottom of the potential energy well of the dipole traps, we can approximate the energy as a simple harmonic oscillator. The trap frequency is the frequency at which atoms oscillate in this simple

harmonic oscillator potential energy well. The light forming the traps goes through an acousto-optic modulator (AOM), as a method of frequency control. We modulate the intensity of the laser by modulating the frequency driving the AOM. The AOM is essentially a fast shutter [13]. We turn on and off the light of the trap walls at different frequencies until we reach a frequency where the atoms start spilling out of the traps. This frequency is twice the trap frequency. The reason it is twice the frequency is that in one oscillation the atoms bounce off both walls of the trap, so the frequency at which we raise and lower the walls must be divided by two.

3.2 Experimental Setup of the Imaging System

3.2.1 Overview of the Imaging System

The transfer from the MOT to the dipole traps is done on the order of ~10 milliseconds, while the expected lifetime of the trap is ~100 milliseconds. As these are such short time spans, we must capture frames on a very short time scale. A Basler piA640-210gm area scan high speed camera is used in conjunction with a photodiode to monitor the atoms. The camera takes 210 frames per second in black and white and communicates with the computer via Ethernet cable. The Ethernet cable is connected to a NI PCIe-8231 Gigabit Ethernet Interface Board which was installed in the computer.

The photodiode was constructed by previous Cal Poly students and is connected to a National Instruments CB-68LP board which is read by the computer via a NI PCI-6014 data acquisition board to acquire voltage readings. The following is a description of the photodiode construction which has not been summarized elsewhere. The photodiodes were primarily constructed by David Gilbert and Troy Kuersten, and the details are documented in their laboratory notebooks.

3.2.2 Construction of Photodiode

The parts required to construct one photodiode are one 10 kΩ resistor, one variable resistor, two 0.1 µF capacitors, one 15 pF capacitor, one 8-pin connector, one 1-pin connector, one small breadboard, one BNC connector, one mini-Dimm (Dual in-line memory module) connector, and one photodiode chip. The mini-Dimm part number is CP-1235-ND ordered from Digi-Key. The photodiode chip used in all lab photodiodes is a UDT-555D ordered from OSI Opto-Electronics. The chip contains the photodiode as well as an operational amplifier. Note that mini-Dimms are used because regular Dimms are too large for our setup.

The box that contains all the photodiode components was purchased, but needed to be machined. Holes for the photodiode chip, power supply connector, BNC, and post were drilled into the box at the machine shop in the Cal Poly Physics Department. The specifications of the box are illustrated in Figure 5. The circuit diagram for the photodiode is shown in Figure 6. Note that the connection for photovoltaic mode is used.

After the chip components have been installed on the breadboard, the BNC and mini-Dimm connectors are placed in the appropriate holes sized for them on the box. Then, the chip is wired to the proper connectors on the BNC and Dimm connectors and the photodiode is attached to the 8-pin connector through the remaining hole in the box. The box is then closed and fastened to an optical post.

To test the completed photodiode, first check all connections on the chip using a digital multimeter to ensure they are properly connected. Then, check the soldering connections to the BNC and Dimm connectors. Last, check all connections on the chip that should not be connected using the digital multimeter. Since the output voltage from the photodiode is proportional to

power, the ratio can be calibrated by comparing measurements to a calibrated power meter. By taking voltage readings at various power levels, one can determine the conversion factor between power and voltage. This conversion factor can be changed by altering the gain resistor value inside the photodiode.
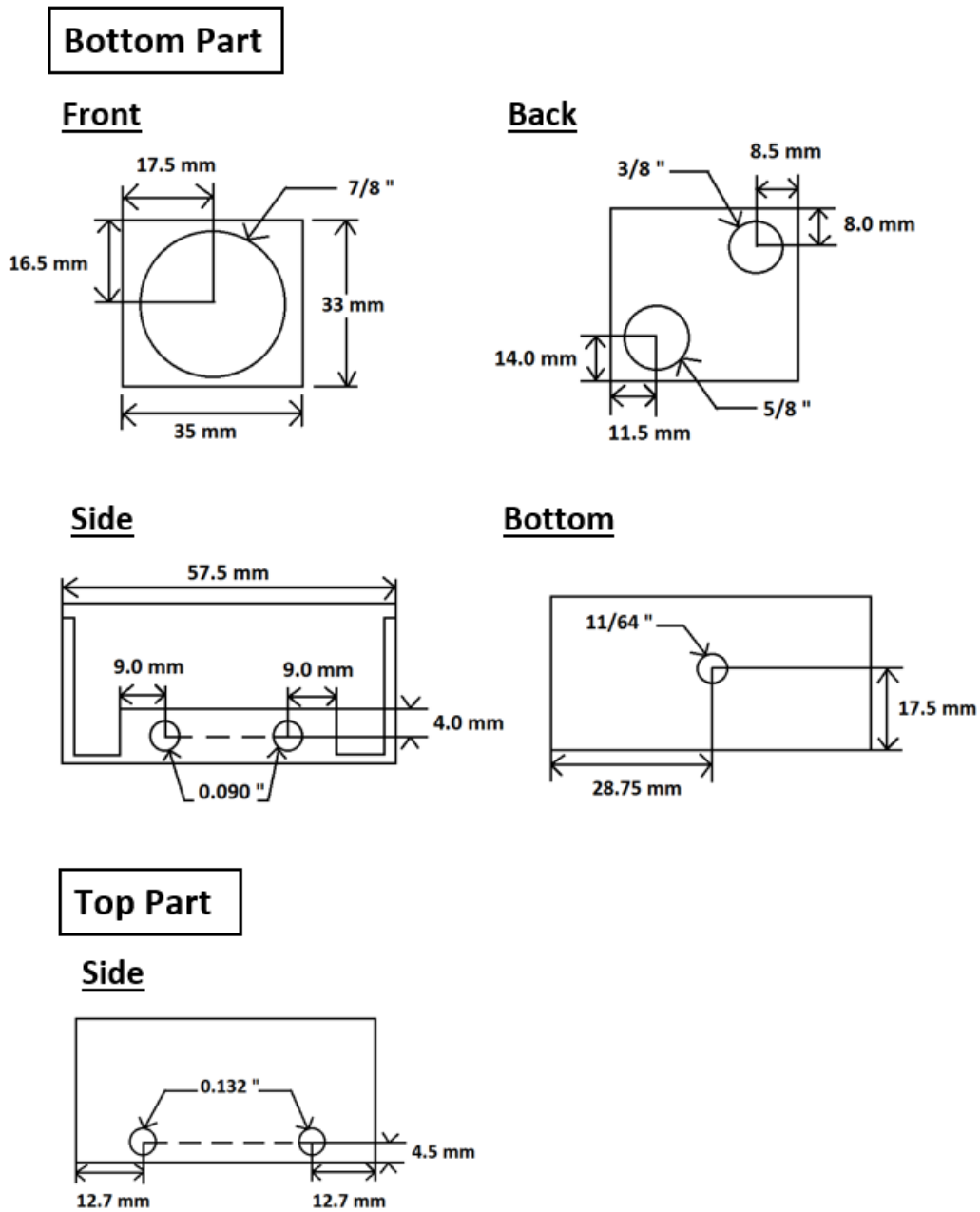
Figure 5: Machining specifications for photodiode box based on Troy Kuersten's notes
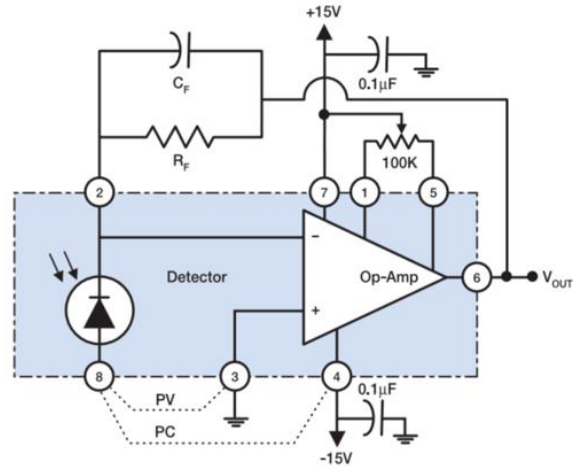
Figure 6: Circuit diagram of photodiode [13]

3.2.3 Optical Setup of the Camera and Photodiode

A lens was placed in front of the camera in order to create a focused image of the MOT on the

CCD array. The camera is positioned 17.7 cm from the center of the MOT. The MOT is at a

height of 189.7 mm, and the camera is placed at an angle up from the horizontal, as shown in
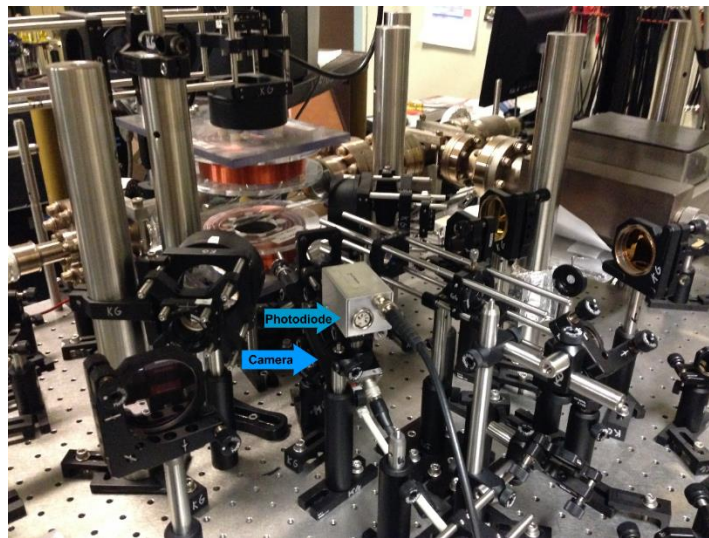
Figure 7.

Figure 7: The optical setup with the camera and photodiode

The distances between the camera and the MOT were used to calculate the correct focal length of the lens. A diagram of the setup for the calculation is shown in Figure 8. To find the correct lens focal length, we solve for focal length as a function of the image distance s' given in Equation 6.

$$\frac{1}{f} = \frac{1}{s} + \frac{1}{s'} \tag{6}$$

Using the fact that s = 17.7cm – s', we solve to get

$$f(s') = \frac{(17.7 \; cm - s') \; s'}{17.7 \; cm} \tag{7}$$

We wanted the setup to be compact, so we solved for as small of a focal length as possible. The smallest coated NIR lens we have is a 25.4 mm focal length lens, and we found that 25.4 mm was an appropriate size for the focal length. With this focal length, the distance between the camera and lens (s') was found to be 2.96 cm. The lens used is an AR coated LA9151-B plano-convex lens by Thorlabs.
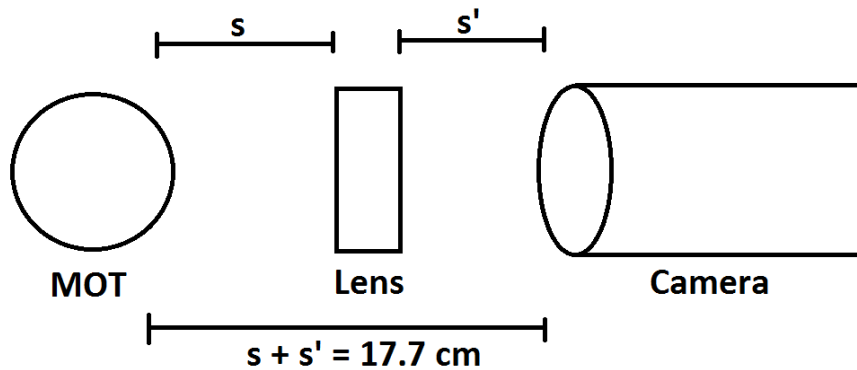

Figure 8: Setup for calculation of the focal length

The setup has a z translation stage (SM1Z by Thorlabs) so that slight adjustments in lens position may be made if necessary. These slight adjustments allow us to focus on a certain plane (slice) of

16

the MOT. The camera is mounted to a cage system to keep the camera and lens aligned properly. These properties can be seen in Figure 9. The photodiode has a similar setup with a lens shown in Figure 10. The rate at which photons hit the photodiode is reduced by the solid angle covered by the collection lens, as described in Section 3.1. The camera and photodiode are placed at angles that minimize any light reflecting from the lasers off the walls of the vacuum chamber, as seen in Figure 7.
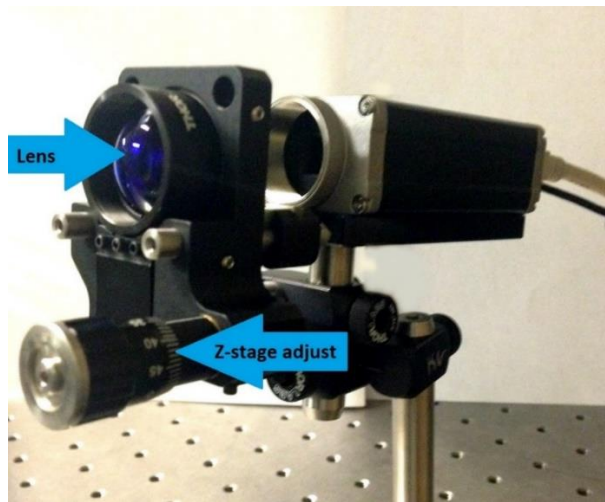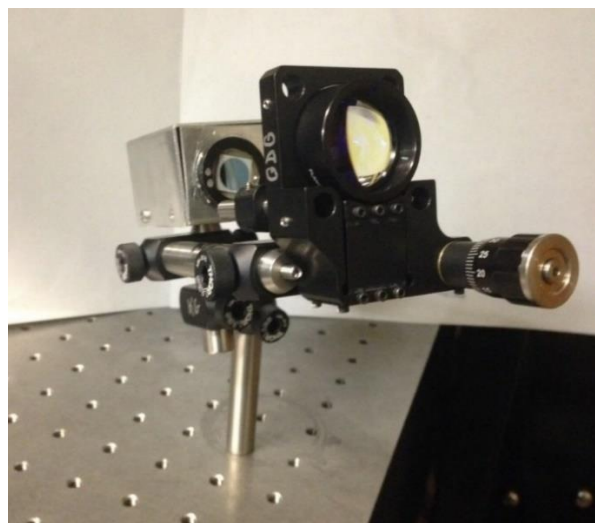

Figure 9: The camera with z-stage and lens

Figure 10: The photodiode with z-stage and lens

3.2.4 LabVIEW Code for Collecting and Saving Data

I wrote a LabVIEW program that captures and saves camera frames and photodiode readings. The block diagram is shown in Figure 11 and the front panel is shown in Figure 12. LabVIEW version 8.2 Professional Development System was used along with National Instruments IMAQ 6.2.4 which facilitates camera configuration and image acquisition. Every 4.7 milliseconds that the program is running, a camera frame of 640x480 pixels is stored in an array in a while loop, which is shown up close in Figure 13. At the same time, photodiode voltage readings are read from the NI PCI-6014 data acquisition board and stored to a separate array. When the program ends, the camera array is parsed and stored in a series of text files named by frame number. This is done in a case structure, shown in Figure 14, which is true when the program stops acquiring frames. Since each text file contains 640x480, or 307,200 readings, running the program for even only a few seconds produces a large amount of data. The photodiode readings are stored in a separate text file.

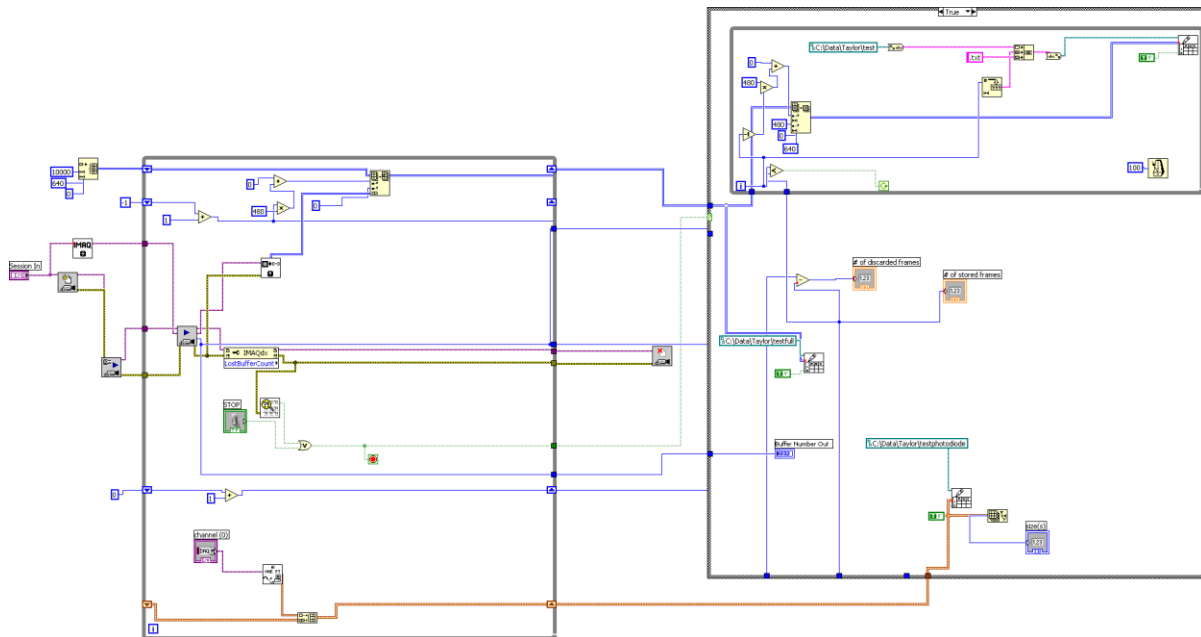Figure 11: Block diagram for program that captures camera frames and photodiode voltages

18

Figure 12: Front Panel for program that captures camera frames and photodiode voltages

Figure 13: While loop that acquires camera frames and photodiode readings and stores them in arrays

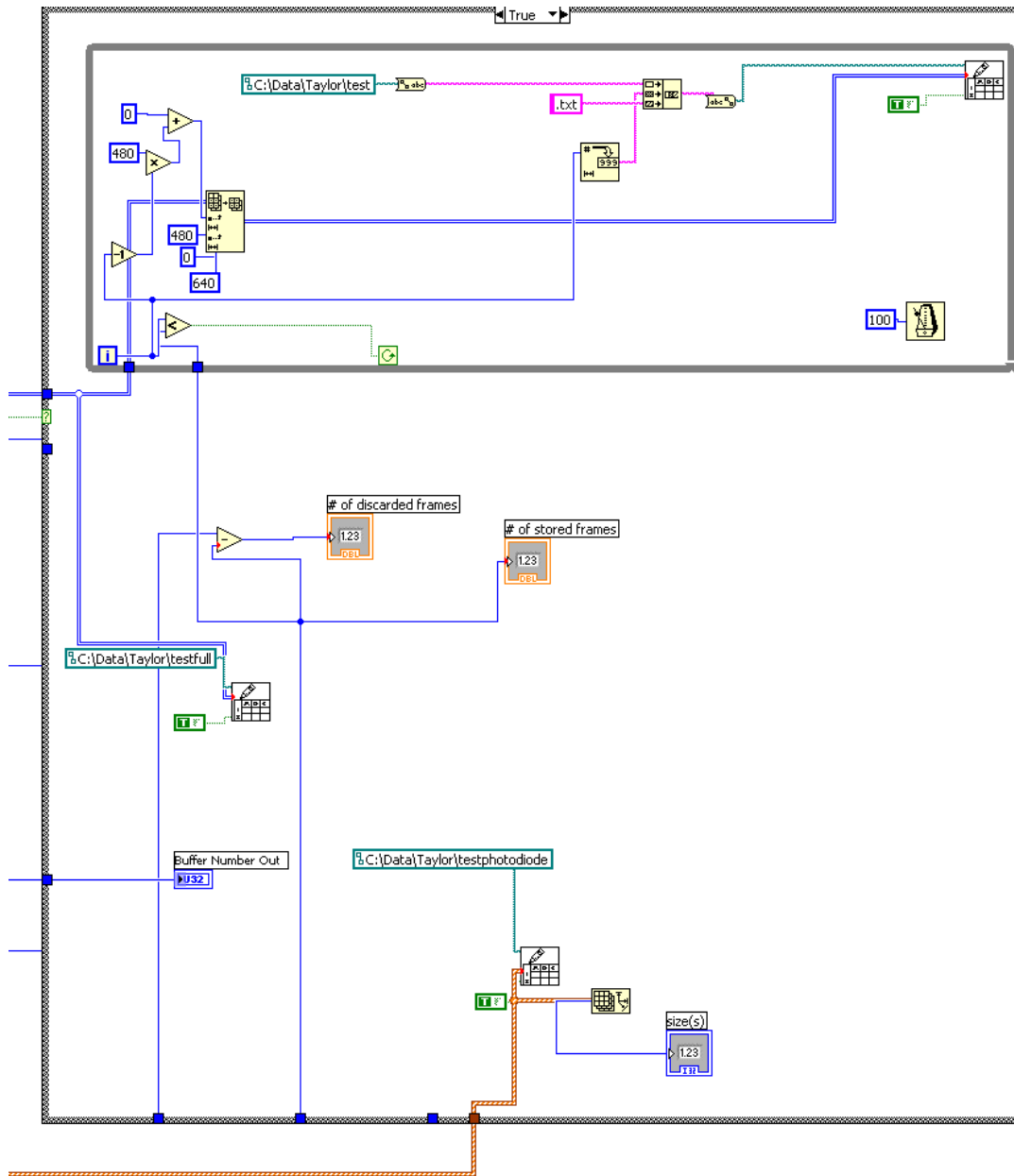Figure 14: Case structure that parses and saves the image and photodiode arrays once acquisition has ended

I wrote a separate program to read all the text files back in numerical order and display them as a video. The block diagram is shown in Figure 15 and the front panel is shown in Figure 16. A for loop is used to iterate through each frame and the display is shown with an intensity graph since

20

each text file contains an array of numbers that are proportional to intensity. The text files may also be opened and viewed individually.
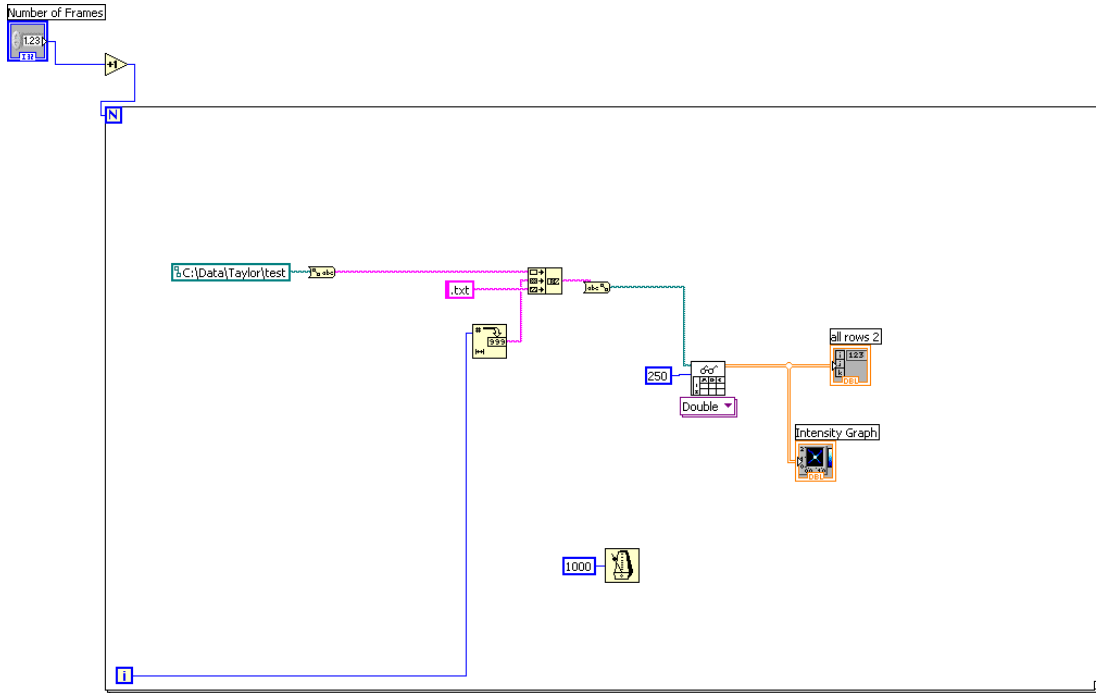

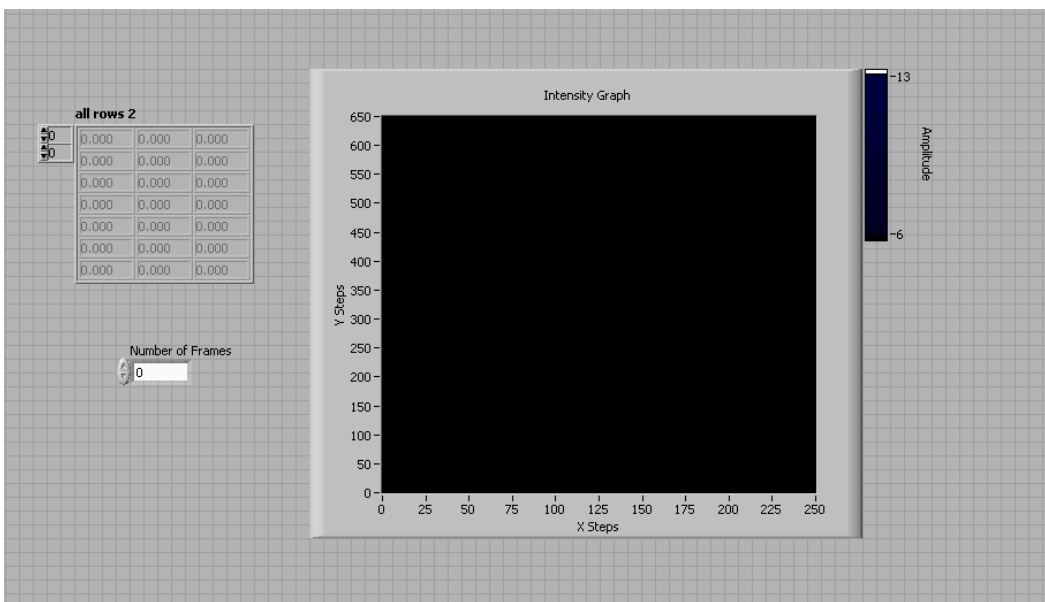Figure 15: Block diagram for program that reads saved frames and displays them

Figure 16: Front panel for program that reads saved frames and displays them

21

3.3 Troubleshooting of Imaging System

3.3.1 Installation of Imaging System Software

Quite a bit of troubleshooting went into this project, as is often the case when programming. When first testing the Basler high speed camera, it was cooperating on Pylon Viewer (the free software downloaded from Basler), but was timing out in NI MAX. After some research on the internet, I found a solution. Open NI Max, select the camera, click on "Camera Attributes", "Expand All", and then under "Test Packet Parameters" make sure that "Test Packet Enabled" is unchecked (which it wasn't). Then, under "Acquisition Attributes" set the packet size to 1500 bytes. To get a full packet we would normally need 8000 bytes, but this caused an error.

Once the camera was working correctly in NI MAX, I attempted to install IMAQ on the computer. IMAQ is the group of VI's used to facilitate communication between the computer and camera. I was installing IMAQ from a Vision Acquisition 8.5.1 disk from National Instruments. However, after the installation, the VI's were not showing up under "Vision and Motion" in the functions palette in LabVIEW, as they should. I called National Instruments and was reassured that LabVIEW 8.2 is compatible with IMAQ 4.0 (which was the version I was attempting to install) on Windows XP. National Instruments instructed me to uninstall and re-install. I did this multiple times with multiple versions of IMAQ and it never cooperated. Fortunately, a different computer in the lab already had IMAQ successfully installed in LabVIEW, and was already connected to the board required to read the photodiode voltages. The only component missing was the Ethernet board required to communicate with the camera. We installed the NI PCIe-8231 Gigabit Ethernet Interface on that computer, and the computer was fully equipped for the purpose of the program.

3.3.2 Programming the Image Acquisition Code

In the first versions of the program, I truncated the image array under the assumption that storing less data on each while loop iteration would make the program more efficient. For example, instead of storing the full 640x480 pixels, I thought that it would increase performance to only capture 100x100. I started out with 3x3 as a basic test, and the program was storing about 85% of the frames sent by the camera into the array. The good news was that no matter how many frames were stored, they were always in packets of 3x3. When I increased the size to 100x100, the program was only storing about 28% of the frames. Once again, integer packets of 100x100 frames were always stored, but this rate was unacceptable.

I found that certain attributes of the program were drastically hindering the speed and lowering the frame storage rate. I had the live images from the camera as well as the running time of the program displaying on the front panel while the program was running. Removing both these unnecessary items increased the frame storage rate significantly. Additionally, I found that truncating the array from 640x480 to 100x100 before storing the array was actually slowing down the program, presumably because truncating the array on each while loop iteration (every 4.76 ms) requires more processing time. Storing all the values (640x480 per frame) increased the frame storage rate.

The program is currently essentially streamlined; there are no unnecessary items on the front panel, and the program is simply storing all raw data. At this point, it stores an average of 97% of the frames. I thought that perhaps storing the photodiode data simultaneously was slowing down the program, but this proved incorrect upon trial. Removing photodiode voltage readings made no difference at all.

23

I wrote a simple program that reveals the raw frame rate that LabVIEW receives from the camera. On certain runs of the program, the frame rate is 210 as it should be, but other times it is 202, or 207 for example. This is in an unrestrained while loop that simply takes the max frame rate from the camera (no while loop timing is involved). This program does not store frames, yet it does not receive a consistent rate from the camera. This is significant because missing one frame could mean the difference between a 4.76 ms gap and a 9.52 ms gap, which is a large difference considering the time scales we are dealing with. To make matters worse, we don't know which frames are being skipped. Checking which frames are lost slows down the program too much and decreases the frame capture rate.

This remaining problem is tricky because the program is storing 210 frames part of the time, but not consistently. This is difficult to deal with because the code is not fundamentally changing between runs, so one would expect the code to consistently retrieve the same frame rate each run. I think that this could be due to the computer interrupting at random times. Next quarter, I will look into a method to stop this from happening. The goal for the future is to ensure that 210 frames are consistently captured. Additionally, I will make sure that the program begins storing frames only when it receives a 5 volt input trigger signal.

Conclusion

To increase computing power for numerous practical advantages, scientists are actively researching the field of quantum computing. Neutral atom quantum computing is a promising avenue towards building a quantum computer that satisfies four of the five DiVincenzo criteria. This involves a magneto-optical trap to cool the atoms and move them to a cloud in the center of a vacuum chamber. Then laser light will be shone through an array of pinholes to trap the atoms in an array of dipole traps. In order to ensure the atoms are trapped, I have set up an imaging

system that consists of a high speed camera and a photodiode. The imaging system is to be used to determine whether the atoms were successfully trapped, calculate how many were trapped, and measure the temperature of the trap, the trap lifetime, and the trap frequency. In the future, I will fix the last bug that is preventing the program from getting a consistent frame rate, and have the program store frames only when it has received a trigger signal. The system will be tested and used as soon as the MOT up and running again. After this, we will have a working imagining system in place that will allow us to check the feasibility of dipole traps formed behind a pinhole for use in neutral atom quantum computing.

References

[1] Moore, Gordon E. "Cramming more components onto integrated circuits." *Electronics*, vol. 8, no. 8, (1965).

[2] "IBM research determines atomic limits of magnetic memory." *Database and Network Journal, Academic OneFile*, 42.1, (2012).

[3] Brennen, Gavin, Ivan Deutsch, and Poul Jessen. "Quantum Computing with Neutral Atoms in an Optical Lattice." *Fortschr. Phys*. 48, (2000).

[4] DiVincenzo, David. "The Physical Implementation of Quantum Computation." *IBM T.J. Watson Research Center*, (2008).

[5] Grimm, Rudolf, Matthias Weidemüller, and Yurii Ovchinnikov. "Optical dipole traps for neutral atoms." *Adv. At. Mol. Opt. Phys.* 42, 95, (2000).

[6] "Neutral Atom Approaches to Quantum Information Processing and Quantum Computing." *A Quantum Information Science and Technology Roadmap,* (2004).

[7] Gillen-Christandl, Katharina, and Bert Copsey. "Polarization-dependent atomic dipole traps behind a circular aperture for neutral-atom quantum computing." *Physical Review.* A 83.023408 (2001).

[8] Christandl, Katharina, Glen Gillen, and Shekhar Guha. "Optical dipole traps for cold atoms using diffracted laser light." *Physical Review*. A 74.013409 (2006).

[9] Wright, Edward. "Doppler Shift." *UCLA astro*. (2002).

[10] Christandl, Katherina. "Advancing Neutral Atom Quantum Computing: Studies of One-Dimensional and Two-Dimensional Optical Lattics on a Chip." *The Ohio State University,* (2005).

[11] "N-BK7 Plano-convex Lenses (650-1050nm) Features"

http://www.thorlabs.us/newgrouppage9.cfm?objectgroup_id=3280&pn=LA1951-B

[12] Brzozowski, Tomasz. "Time-of-flight measurement of the temperature of cold atoms for short trap-probe beam distances." *Journal of Optics B: Quantum and Semiclassical Optics*. 62-66 (2002).

[13] Lewandwoski, H.J., D.M. Harber, D.L. Whitaker, and E.A. Cornell. "Simplified System for Creating a Bose-Einstein Condensate." *National Institute of Standards and Technology and University of Colorado Department of Physics.*

[14] Photops Photodiode-Amplifier Hybrids Manual